Cyclotron Resonance and the Cohen Nonellipsoidal Nonparabolic Model for Bismuth*

R. J. DINGER AND A. W. LAWSON
Department of Physics, University of California, Riverside, California 92502
(Received 8 September 1969)

An equation for the cyclotron effective mass in the Cohen nonellipsoidal nonparabolic (NENP) model for Bi is derived for an arbitrary direction of the magnetic field. This equation is compared with the previously published cyclotron-resonance data of Kao and of Edel'man and Khaikin (EK). In both cases very good agreement between experiment and the NENP model is found for the binary-plane data, and the fit is clearly superior to that of the ellipsoidal nonparabolic (ENP) model; in the remaining orientations the experimental points suffer more scatter, but seem to fit the NENP model better than the ENP model. The quantity η, as defined by Bhargava, is recalculated using the m^* values of EK rather than those of Kao. The value $\eta=1.13\pm0.05$ is found, confirming the NENP model.

I. INTRODUCTION

IT is well established experimentally[1] that the electron Fermi surface of Bi consists of three equivalent highly elongated quasiellipsoids having one principal axis parallel to the binary axis and the other two principal axes tilted approximately 6 degrees from the bisectrix and trigonal axes. The shape of each of these quasiellipsoids has been the object of many experimental[1] and several theoretical[2,3] researches. The $\mathbf{k}\cdot\mathbf{p}$ calculation of Cohen[2] predicts that the electron dispersion relation is

$$\frac{p_1^2}{2m_1}+\frac{p_2^2}{2m_2}+\frac{p_3^2}{2m_3}=E\left(1+\frac{E}{E_g}\right)-\left(\frac{p_2^2}{2m_2}\right)^2\frac{1}{E_g}, \quad (1)$$

where 1, 2, 3 refer to the principal-axis system of the quasiellipsoid, the m_i are effective masses at the bottom of the conduction band, and E_g is the band gap.[4,5] The quartic term in p_2 gives rise to a Fermi surface (obtained by setting $E=E_F$), which is distorted at large values of p_2 from an ellipsoid. Equation (1) represents a band having nonparabolic dispersion in the p_1 and p_3 directions and parabolic dispersion in the p_2 direction. Cohen's model thus predicts a nonellipsoidal Fermi surface and a nonparabolic energy band and is known as the NENP model. Another model frequently used is due to Lax[6] and has a dispersion relation identical with Eq. (1), except that the quartic term is absent. This model then has an ellipsoidal Fermi surface but nonparabolic bands and is known as the ENP model. The nonparabolicity of the electron energy bands as predicted by the NENP and ENP models has been well verified experimentally.[7–13] The nonellipsoidality is still open to question. Many experiments[1,14–18] seem to agree well with an ellipsoidal Fermi surface; however, the experimental error in Refs. 14–18 would prevent an unambiguous detection of any nonellipsoidal effects predicted by the NENP model. The experimental errors in the de Haas–van Alphen experiment of Bhargava[19] are small enough so that nonellipsoidal effects should appear if they exist; Bhargava concludes that the Fermi surface is very nearly ellipsoidal. It appears, however, that this conclusion is not justified on the basis of his data, which actually seem to support the NENP model. We discuss this point in detail in Sec. IV.

Besides the work of Bhargava,[19] there are two other experiments[20,21] that have been done with the necessary precision to show up nonellipsoidal effects; both are cyclotron resonance. Qualitatively, the angular variation of the cyclotron effective masses seems to agree with the NENP model, but, except in one case (in Kao's paper), a quantitative comparison with Eq. (1) has not been carried out. The basic reason has been the

* Work supported by a grant from the National Science Foundation.

[1] For a complete list of references see W. S. Boyle and G. E. Smith, in *Progress in Semiconductors* (John Wiley & Sons, Inc., New York, 1963), Vol. 7.

[2] M. H. Cohen, Phys. Rev. **121**, 387 (1961).

[3] A. A. Abrikosov and L. A. Fal'kovskii, Zh. Eksperim. i Teor. Fiz. **43**, 1089 (1962) [English transl.: Soviet Phys.—JETP **16**, 769 (1963)].

[4] Cohen's original equation contains another parameter, m_2', the effective mass component at the top of the electron valence band. Recent experimental evidence seems to indicate that $m_2\approx m_2'$, and hence we have set $m_2=m_2'$. See Ref. 5 for a discussion of this point.

[5] G. A. Antcliffe and R. T. Bate, Phys. Rev. **160**, 531 (1967).

[6] B. Lax, Rev. Mod. Phys. **30**, 122 (1958); B. Lax, Bull. Am. Phys. Soc. **5**, 167 (1960).

[7] R. N. Brown, J. G. Mavroides, M. S. Dresselhaus, and B. Lax, Phys. Rev. Letters **5**, 243 (1960).

[8] G. E. Smith, Phys. Rev. Letters **9**, 487 (1962).

[9] G. E. Smith, G. A. Baraff, and J. M. Rowell, Phys. Rev. **135**, A1118 (1964).

[10] H. Kunze, Phys. Letters **20**, 469 (1966).

[11] R. T. Bate and N. G. Einspruch, Phys. Rev. **153**, 796 (1967).

[12] W. E. Engeler, Phys. Rev. **129**, 1509 (1963).

[13] R. N. Brown, J. G. Mavroides, and B. Lax, Phys. Rev. **129**, 2055 (1963).

[14] D. Weiner, Phys. Rev. **125**, 1226 (1962).

[15] Y. Eckstein and J. B. Ketterson, Phys. Rev. **137**, A1777 (1965).

[16] D. N. Reneker, Phys. Rev. **115**, 303 (1959).

[17] M. S. Khaikin and V. S. Edel'man, Zh. Eksperim. i Teor. Fiz. **47**, 878 (1964) [English transl.: Soviet Phys.—JETP **20**, 587 (1965)].

[18] G. E. Smith, L. C. Hebel, and S. J. Buchsbaum, Phys. Rev. **129**, 154 (1963).

[19] R. N. Bhargava, Phys. Rev. **156**, 785 (1967).

[20] Y. H. Kao, Phys. Rev. **129**, 1122 (1963).

[21] V. S. Edel'man and M. S. Khaikin, Zh. Eksperim. i Teor. Fiz. **49**, 107 (1965) [English transl.: Soviet Phys.—JETP **22**, 77 (1966)], hereafter EK.

lack of an expression for the cyclotron effective mass for an arbitrary direction of the applied magnetic field **H** for the NENP model. Such a quantitative comparison would be useful for several reasons: (i) It would help verify or disprove the NENP model; (ii) it would possibly allow one to establish more clearly the value of E/E_g in pure Bi, which has ranged in the literature from 0.5 to 2.

In this paper, we derive an equation for m^* from Eq. (1) for an arbitrary direction of **H** and make a comparison with the previously published data of Kao[20] and Edel'man and Khaikin.[21] We find that the reasonably good agreement of their data with the NENP model, coupled with a reinterpretation of Bhargava's[19] results, establishes the validity of Cohen's NENP model for Bi. We also discuss the possible application of the NENP model towards explaining the anomalous electron spin splitting found in the high-field Shubnikov-de Haas data.

II. THEORY

The ultimate goal is an equation for $m_j^*(\alpha,\beta)$, where α and β are angles that define the field direction with respect to the crystallographic axes (Fig. 1). The subscript on m_j^* refers to one of the three quasiellipsoids; $j=$I refers to the quasiellipsoid whose p_2 and p_3 principal axes differ only by the tilt angle θ_t from the bisectrix and trigonal axes, and $j=$II, III refer to the quasiellipsoids obtained by rotations of the $j=$I quasiellipsoid by $+120$ degrees and -120 degrees, respectively, about the trigonal axis. First, however, it is convenient to obtain $m^*(\theta,\Omega)$, where θ and Ω are defined similarly to α and β, respectively, except that θ and Ω are measured with respect to axes p_1, p_2, and p_3, the principal-axis system of the quasiellipsoid. We then compute the transformations from the principal-axis system of each quasiellipsoid to the crystallographic-axis system. This procedure is the reverse of the procedure suggested by Kao; his approach was to transform Eq. (1) to the crystallographic-axis system and then to attempt to compute m^*. The equation thus obtained, however, is highly unamenable to solution for m^*, since it contains a large number of quartic cross terms in p_1, p_2, and p_3. The procedure used here avoids this problem.

For the surface of Eq. (1), the cyclotron effective mass is related to the Fermi surface geometry by

$$m^*=(1/2\pi)[\partial \mathfrak{A}(E)/\partial E], \tag{2}$$

where $\mathfrak{A}$ is the extremal cross-sectional area of the Fermi surface perpendicular to H. We note that since Eq. (1) possesses inversion symmetry and gives a surface that is nonreentrant, it makes no difference whether we compute $(\partial \mathfrak{A}_{\rm ext}/\partial E)$ or $(\partial \mathfrak{A}/\partial E)_{\rm ext}$ ("ext," for "extremal," has been supplied for clarity), because both will give the same result. The latter quantity is the customary definition of the cyclotron effective mass,

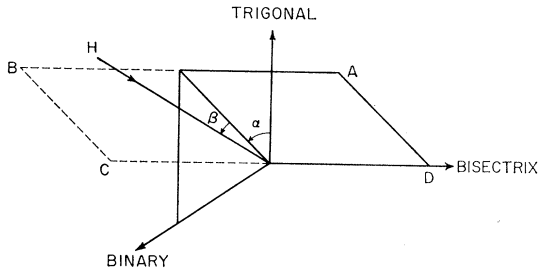

FIG. 1. Definition of magnetic-field direction. Plane ABCD is the trigonal-bisectrix plane rotated counterclockwise by angle α as one looks along bisectrix axis in negative direction. Angle β is an angle in this rotated plane.

but the former is easier to compute, and hence we use it in Eq. (2). In order to obtain $\mathfrak{A}(E)$, we need to compute the area enclosed by the trace of the surface of Eq. (1) upon that plane perpendicular to **H** which passes through the origin. To this end we compute the transformation that aligns the p_3 axis along **H**. This transformation requires (i) a rotation by θ about the p_2 axis and (ii) a rotation by Ω about the new p_1 axis. Taking the inverse of this transformation gives the equations

$$p_1=p_1'\cos\theta+p_2'\sin\Omega\sin\theta+p_3'\cos\Omega, \tag{3a}$$

$$p_2=p_2'\cos\Omega-p_3'\sin\Omega, \tag{3b}$$

$$p_3=-p_1'\sin\theta+p_2'\sin\Omega\cos\theta+p_3'\cos\theta\cos\Omega, \tag{3c}$$

where the primes refer to the coordinate system whose p_3' axis is aligned along **H**. Substituting (3) into (1) and setting $p_3'=0$ we obtain

$$A(p_2')^4+B(p_2')^2+C(p_1')^2+Dp_2'p_1'-F=0, \tag{4}$$

where

$$A=(\cos^4\Omega)/4m_2^2E_g,$$

$$B=\tfrac{1}{2}[(\cos^2\Omega)/m_2+(\sin^2\Omega\sin^2\theta)/m_1+(\cos^2\theta\sin^2\Omega)/m_3],$$

$$C=\tfrac{1}{2}[(\cos^2\theta)/m_1+(\sin^2\theta)/m_3],$$

$$D=\sin\Omega\sin\theta\cos\theta\,(m_1^{-1}-m_3^{-1}),$$

and

$$F=E(1+E/E_g).$$

The area enclosed by Eq. (4) then is the area required for Eq. (2). Computing this area, we obtain

$$\mathfrak{A}=8[(A/C)(G_++G_-)]^{1/2}\times[G_-K(k)+2(G_+-G_-)\epsilon(k)], \tag{5}$$

where

$$G_\pm=\pm\left(\frac{D^2-4CB}{8CA}\right)+\frac{1}{2}\left[\left(\frac{D^2-4CB}{4CA}\right)^2+\frac{4E(1+E/E_g)}{A}\right]^{1/2},$$

and

$$k=[G_+/(G_++G_-)]^{1/2}.$$

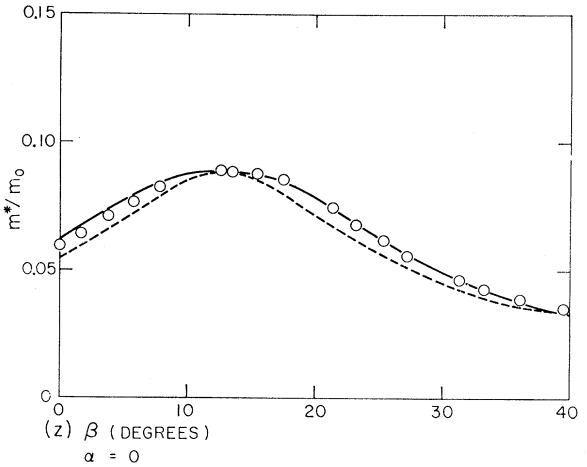

FIG. 2. Angular variation of the electron cyclotron mass m_{II}^* ($=m_{II}^*$) for **H** in the binary plane. The solid curve is computed from the NENP model [Eq. (7)] and the dashed curve from the ENP model [Eq. (8)] with $E/E_g=5/3$. The experimental points and the m_i used for the theoretical curves are from Ref. 21. α and β refer to Fig. 1.

K and ϵ are complete elliptic integrals of the first and second kind, respectively. The following relation[22] is useful in reducing the integral obtained for the area to elliptic integrals:

$$\int_0^g [(f^2+z^2)(g^2-z^2)]^{1/2}dz=\tfrac{1}{3}(f^2+g^2)^{1/2} \times[f^2K(r)+2(g^2-f^2)\epsilon(r)], \quad (6)$$

where $r=g(f^2+g^2)^{-1/2}$. Taking the derivative of Eq. (5) with respect to E, redefining some of the constants, and substituting into Eq. (2) yields, after lengthy algebra,

$$m^*(\theta,\Omega)=\left(\frac{2m_1m_2m_3}{m_3\cos^2\theta+m_1\sin^2\theta}\right)^{1/2}\frac{(1+2E/E_g)K(x)}{\pi b^{1/4}\cos\Omega}, \quad (7)$$

where

$$b=(E/E_g)(1+E/E_g)+\nu^2,$$

$$\nu=\frac{(m_2\tan^2\Omega/\cos^2\theta)+(m_3+m_1\tan^2\theta)}{2(m_3+m_1\tan^2\theta)},$$

$$x=(1+\tau)^{-1/2},$$

and

$$\tau=(\sqrt{b}+\nu)/(\sqrt{b}-\nu).$$

The transformations to the crystallographic-axis system are derived in the Appendix, and are given by Eqs. (A4) and (A5). To compute $m_j^*(\alpha,\beta)$, the values of Ω and θ are obtained from these equations and substituted in Eq. (7).

The expression for $m^*(\theta,\Omega)$ for the ENP model can be obtained from Eq. (7) by letting all E/E_g, *except* the E/E_g appearing in the numerator in the factor $(1+2E/E_g)$, go to zero. We give the resulting equation for reference:

$$m_{\mathrm{ENP}}^*(\theta,\Omega)=\left[\frac{m_1m_2m_3}{m_2\sin^2\Omega+\cos^2\Omega\ (m_3\cos^2\theta+m_1\sin^2\theta)}\right]^{1/2} \times(1+2E/E_g). \quad (8)$$

III. COMPARISON WITH CYCLOTRON-RESONANCE EXPERIMENTS

In this section we compare the cyclotron-resonance data of EK and Kao with Eq. (7). Figure 2 reproduces the data of EK for m_{II}^* ($=m_{III}^*$) for **H** in the binary plane, along with predictions of the two models. The agreement with the NENP model is very good. Since E/E_g is a parameter in Eq. (7), by finding the best fit to the experimental points it was hoped that an accurate value of E/E_g could be obtained. Unfortunately, the angular variation of m^* is relatively insensitive to changes in E/E_g, and almost all one can state is that the generally accepted value[13] for E/E_g in pure Bi of 5/3 fits the data well. We note that the data which EK present for m_I^* for **H** in the binary plane do not extend more than $\pm45°$ beyond the bisectrix axis, whereas deviations from the ENP model occur only within 10° of the trigonal axis. Hence, we can make no comparison with Eq. (7) for m_I^*.

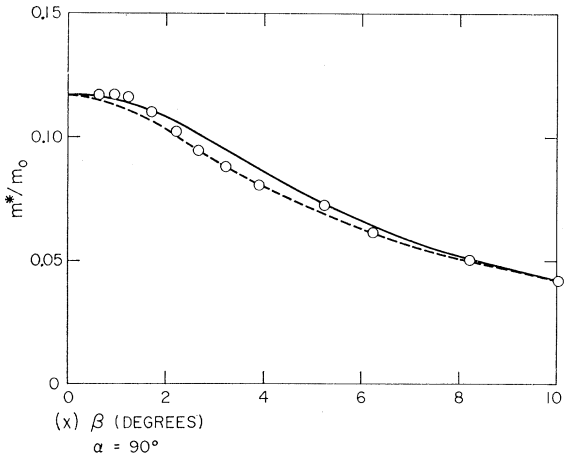

FIG. 3. Angular variation of the electron cyclotron mass m_I^* for **H** in the trigonal plane. The solid curve is computed from the NENP model [Eq. (7)] and the dashed curve from the ENP model [Eq. (8)] with $E/E_g=5/3$. The experimental points and the m_i used for the theoretical curves are from Ref. 21. α and β refer to Fig. 1.

Figure 3 presents the data of EK for m_I^* for **H** in the trigonal plane, along with the predictions of the two models. Although the experimental points deviate from the ellipsoidal model near the binary axis in a manner suggested by the NENP model, the remaining points

[22] I. S. Gradshteyn and I. M. Ryzhik, *Table of Integrals, Series, and Products* (Academic Press Inc., New York, 1965), p. 249.

fit the ellipsoidal model, except near 5 degrees. The only conclusion that can be made is that apparently the scatter of the points is larger than the percentage difference between the two models. For m_{II}^* and m_{III}^* the experimental points are limited and do not extend in those directions where deviations are expected; hence, we can make no comparison with the NENP model.

The third orientation used by EK placed the normal to the sample parallel to the p_2 axis of the principal-axis system of ellipsoid I, i.e., the surface plane of the sample is the bisectrix plane rotated by θ_t about the binary axis. In this orientation Eq. (7) predicts an elliptical angular variation of m_I^*. Within the experimental error EK's data in this orientation fit an ellipse very well, as Fig. 5A in their paper indicates. The ENP model also predicts an elliptical variation in this plane, so that the good agreement with the NENP model does not imply that we have distinguished the NENP model from the ENP model for this case. The good agreement does imply that the NENP model is consistent with experiment in this plane. We note that EK present no experimental points for m_{II}^* and m_{III}^* for this orientation.

It is perhaps questionable whether a detailed comparison with the data of Kao should be attempted. EK state that the deviations from an ellipsoidal shape observed by Kao are within his limits of error; presumably, EK take the error limits as $\pm 10\%$, which is what Kao states for the cyclotron effective mass values for **H** along the three quasiellipsoid principal axes. However, we believe, as Kao states, that the percentage error associated with the angular variation in some cases is much lower than 10%. At any rate, we attempt to draw conclusions only in those cases in which the scatter seems to be within the error limits required to observe the nonellipsoidal effects.

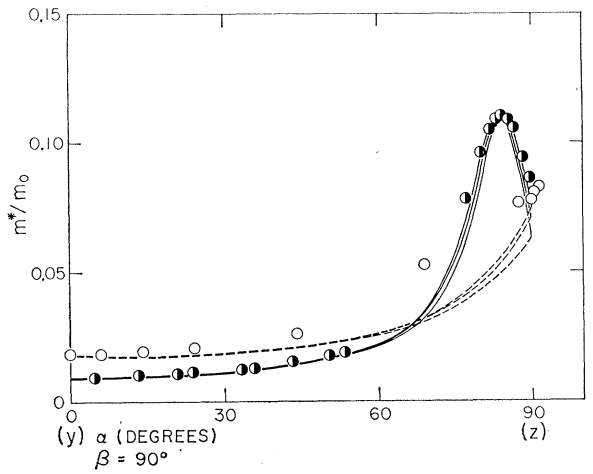

FIG. 4. Angular variation of the electron cyclotron mass for **H** in the binary plane. The solid curves and the points ◑ are for m_I^*; the dashed curves and the points ○ are for m_{II}^* ($=m_{III}^*$). In each case the lower curve is the ENP model [Eq. (8)]; the middle and upper curves are the NENP model [Eq. (7)] with $E/E_g=\frac{1}{2}$ and 5/3, respectively. The experimental points and the m_i used for the theoretical curves are from Ref. 20. α and β refer to Fig. 1.

In the binary plane, Kao was able to compare his data for m_I^* with the NENP model, and the agreement was found to be fairly good. However, he used $E/E_g=0.5$, and we wish to point out that the more generally accepted value of $E/E_g=5/3$ gives better agreement. Figure 4 is a reproduction of Kao's data for **H** in the binary plane showing the better agreement. A higher value of E/E_g would give even slightly better agreement. The experimental points for m_{II}^* ($=m_{III}^*$) are in poor agreement with both models, presumably due to the difficulty mentioned by Kao in identifying the cyclotron-resonance harmonics because of the additional peaks in the power absorption curve.

Figure 5 presents Kao's data for **H** in the bisectrix plane compared with the two models. The NENP model fits the experimental points for m_I^* better than the ENP model, although the scatter is somewhat large. For m_{II}^* and m_{III}^* there is not much difference between the NENP and ENP models, and both compare poorly with the experimental points.

For **H** in the trigonal plane, deviations from the ENP model are expected for angles between **H** and the binary axis of 0 and 60 degrees (considering only the first quadrant). Unfortunately, in these two regions the data of Kao include too few points to draw any positive conclusions. For what it is worth, we have, in Fig. 6, reproduced his data points near the binary axis for m_I^* along with the predictions of the two models. The points seem to fit the NENP model better.

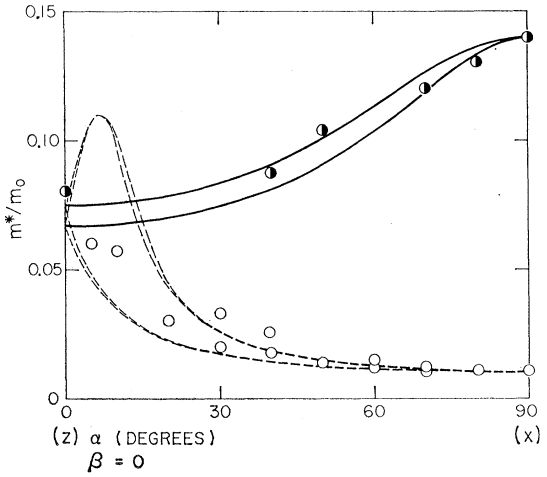

FIG. 5. Angular variation of the electron cyclotron mass for **H** in the bisectrix plane. The solid curves and the points ◑ are for m_I^*; the dashed curves and the points ○ are for m_{II}^* and m_{III}^*. In each case the lower curve is the ENP model [Eq. (8)] and the upper curve is the NENP model [Eq. (7)] with $E/E_g=5/3$. The experimental points and the m_i used for the theoretical curves are from Ref. 20. α and β refer to Fig. 1.

TABLE I. η [Eq. (8)], as calculated using the cyclotron effective masses due to Kao and to Edel'man and Khaikin.

Quasiellipsoid principal axis	Measured[a] area $\mathfrak{A}$, 10^{12} cm^{-2}	m^*/m_0 due to: Kao[b]	m^*/m_0 due to: EK[c]	$\mathfrak{A}/2\pi m^*$, 10^{-3} eV, using m^*/m_0 of: Kao	EK	η, using m^*/m_0 of: Kao	EK
1	18.0±1	0.14 ±0.02	0.120 ±0.003	15.6±2.4	18.2±1.1		
2	1.1±0.01	0.009±0.0009	0.0081±0.0001	14.9±1.5	16.5±0.2	1.02±0.17	1.13±0.05
3	13.7±0.5	0.11 ±0.01	0.088 ±0.002	15.1±1.5	18.9±0.9		

[a] From Ref. 19. [b] From Ref. 20. [c] From Ref. 21.

IV. REINTERPRETATION OF DATA OF REF. 19

Bhargava[19] differentiates between the NENP and ENP models in the following manner. For the ENP model the ratios $(\mathfrak{A}/2\pi m^*)_{1,2,3}$, where 1, 2, 3 refer to **H** along the p_1, p_2, p_3 axes, have the same value. For the NENP model, however, one obtains that

$$\left(\frac{\mathfrak{A}}{2\pi m^*}\right)_{1,3}^{\text{NENP}} = \eta\left(\frac{E}{E_g}\right)\left(\frac{\mathfrak{A}}{2\pi m^*}\right)_2^{\text{NENP}}, \tag{9}$$

where η is obtained from Eqs. (5) and (7) and is given by

$$\eta = 4\sqrt{\gamma}(\sqrt{\gamma}+\tfrac{1}{2})^{-1}(I/K), \tag{10}$$

where

$$I = \frac{1}{3}\left[\frac{1-\lambda^2}{\lambda^2}K(\lambda) - \frac{1-2\lambda^2}{\lambda^2}\epsilon(\lambda)\right],$$

$$\lambda^2 = (\sqrt{\gamma}-\tfrac{1}{2})/2\sqrt{\gamma},$$

and

$$\gamma = [(E/E_g)(1+E/E_g)+\tfrac{1}{4}].$$

Hence, $\eta=1$ implies the ENP model is valid and $\eta\neq 1$ can be interpreted on the basis of the NENP model.

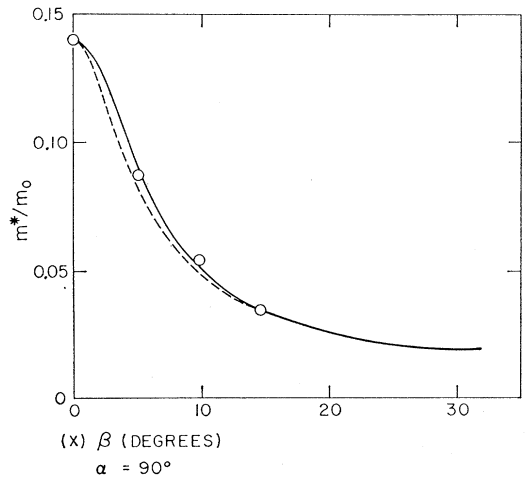

FIG. 6. Angular variation of the cyclotron effective mass for **H** in the trigonal plane. The solid curve is computed from the NENP model [Eq. (7)] for $E/E_g=5/3$ and the dashed curve from the ENP model [Eq. (8)]. The experimental points and the m_i used for the theoretical curves are from Ref. 20. α and β refer to Fig. 1.

The NENP model predicts a η between 1.12 and 1.23 for E/E_g between 0.5 and 2.0.

The bad feature of this method is the need for effective mass values from other experiments. Bhargava used Kao's values of m^* and found that $\eta=1$ within the large experimental uncertainties (Table I), and hence concluded that the Fermi surface is ellipsoidal. Kao's m^* values, however, have the rather large uncertainty of 10%. The more precise m^* values of EK appeared subsequent to Bhargava's work, and it is of interest to recompute η using their effective masses.

The results are summarized in Table I. The value of $\eta=1.13$ obtained using EK's values for m^* corresponds to $E/E_g=0.5$, which is somewhat lower than the accepted value of $E/E_g=5/3$. We feel, however, that a deviation of 13% in η from unity along with the close agreement of $(\mathfrak{A}/2\pi m^*)_1^{\text{NENP}}$ and $(\mathfrak{A}/2\pi m^*)_3^{\text{NENP}}$ supports the NENP model.

V. POSSIBLE APPLICATION OF NENP MODEL TO SPIN SPLITTING

The fairly good agreement between the NENP model and the cyclotron-resonance data, along with the support given the model by Bhargava's data, leads one to consider more closely the theoretical[23,24] and experimental[9] results on the g factor and spin splitting in Bi. For a magnetic field along, say, the p_3 principal axis, the energy levels are given in the ENP model by

$$E(1+E/E_g) = (n+\tfrac{1}{2})\hbar\omega_c + p_3^2/2m_3 \pm \tfrac{1}{2}g\beta_0 H, \tag{11}$$

where

$$\omega_c = eB/(m_1m_2)^{1/2}c, \quad \text{(for this case)}$$

$$\beta_0 = e\hbar/2m_0c,$$

and g is the effective g factor. The calculation of Cohen and Blount[23] using the ENP model gives the result that for most orientations of **H**, $g=2m_0/m_c^*$. By Eq. (11) this value for g gives a spin splitting that is equal to the Landau level spacing (orbital splitting). However, the Shubnikov–de Haas results of Smith, Baraff, and Rowell[9] (SBR) indicate that the spin splitting is about one-third of the orbital splitting in the heaviest mass direction and about 10% larger than the orbital splitting in the light-mass direction. In a subsequent paper Baraff[24] was able to explain the difference between the

[23] M. H. Cohen and E. I. Blount, Phil. Mag. **5**, 115 (1960).
[24] G. A. Baraff, Phys. Rev. **137**, A842 (1965).

spin and orbital splittings theoretically by including the effects of bands other than the two considered in the two-band model. His final equations contain several new parameters and are fairly complicated, and no detailed comparison with the SBR data is attempted; but it is apparent that his calculation explains the experimental results. The main conclusion to be drawn from Baraff's paper is the clear importance of the additional bands.

The relationship and relevance of the SBR measurements and Baraff's model to the present work are as follows. The existence of the p_2^4 in Eq. (1), which is responsible for the fairly good agreement between theory and experiment, is tantamount to including the effects of higher-order bands in the p_2 direction. Given the need for such bands to explain the spin-splitting results, it would be of interest to extend the NENP model to high fields and to determine if it offers a simpler explanation of the spin and orbital splittings than Baraff's model—simpler in the sense that no new parameters would be introduced. Such a procedure may also suggest changes in the NENP model, which would give even better agreement with the cyclotron-resonance data. We are presently undertaking the investigation just outlined.

VI. CONCLUSIONS

We have derived an equation for the cyclotron effective mass as a function of the magnetic-field direction for the Cohen NENP model and have made a comparison with the previously published results of EK and Kao. The excellent agreement of experiment with the NENP model for the binary-plane data of EK argues very convincingly for the validity of the NENP model. The binary-plane data of Kao for m_1^* also fit the NENP model well. The near-bisectrix-plane data of EK, while precise, do not allow a distinction to be made between the two models. The remaining data of both EK and Kao seem subject to more error than the cases already mentioned, but do appear to give a superior fit to the NENP model. In general, a value of $E/E_g=5/3$ gives a consistent fit to the experimental points. The recomputation of η in Sec. IV not only supports the NENP model, but also negates the one case in the literature in which the NENP model is unambiguously shown not to fit experiment. The success of the NENP model in explaining the cyclotron-resonance data suggests that the model may also explain the electron spin splitting at high magnetic fields.

ACKNOWLEDGMENTS

The authors wish to thank Dr. J. C. Shaw and G. S. Cooper for many helpful conversations.

APPENDIX

Let the primed coordinates denote the crystallographic-axis system, and the unprimed coordinates the principal-axis system. It is easily shown that

$$\begin{aligned} p_1&=\cos\phi\, p_1'-\sin\phi\, p_2',\\ p_2&=\sin\phi\cos\theta_t\, p_1'+\cos\phi\cos\theta_t\, p_2'-\sin\theta_t\, p_3', \\ p_3&=\sin\phi\sin\theta_t\, p_1'+\cos\phi\sin\theta_t\, p_2'+\cos\theta_t\, p_3', \end{aligned} \tag{A1}$$

where θ_t is the tilt angle and $\phi=0$, 120, -120 degrees for quasiellipsoids I, II, III, respectively. In the unprimed system, a point a distance r from the origin has the coordinates

$$\begin{aligned} p_1&=r\cos\Omega\sin\theta,\\ p_2&=-r\sin\Omega, \\ p_3&=r\cos\Omega\cos\theta, \end{aligned} \tag{A2}$$

while in the primed system,

$$\begin{aligned} p_1'&=r\cos\beta\sin\alpha,\\ p_2'&=-r\sin\beta, \\ p_2'&=r\cos\beta\cos\alpha. \end{aligned} \tag{A3}$$

Substituting Eqs. (A2) and (A3) into (A1) and solving for $\sin\Omega$ and $\tan\theta$ gives

$$\sin\Omega=-\sin\phi\cos\theta_t\cos\beta\sin\alpha+\cos\phi\cos\theta_t\sin\beta+\sin\theta_t\cos\beta\cos\alpha \tag{A4}$$

and

$$\tan\theta=\frac{\cos\phi\sin\alpha+\sin\phi\tan\beta}{\sin\phi\sin\theta_t\sin\alpha-\cos\phi\sin\theta_t\tan\beta+\cos\theta_t\cos\alpha}. \tag{A5}$$